Operation of Direct Drive Systems: Experiments in Peak Power Tracking and Multi-Thruster Control

IEPC-2013-044

Presented at the 33rd International Electric Propulsion Conference,
The George Washington University • Washington, D.C. • USA
October 6 – 10, 2013

John Steven Snyder* and John R. Brophy†
Jet Propulsion Laboratory, California Institute of Technology, Pasadena, CA 91109

Direct-drive power and propulsion systems have the potential to significantly reduce the mass of high-power solar electric propulsion spacecraft, among other advantages. Recent experimental direct-drive work has significantly mitigated or retired the technical risks associated with single-thruster operation, so attention is now moving toward systems-level areas of interest. One of those areas is the use of a Hall thruster system as a peak power tracker to fully use the available power from a solar array. A simple and elegant control based on the incremental conductance method, enhanced by combining it with the unique properties of Hall thruster systems, is derived here and it is shown to track peak solar array power very well. Another area of interest is multi-thruster operation and control. Dual-thruster operation was investigated in a parallel electrical configuration, with both thrusters operating from discharge power provided by a single solar array. Startup and shutdown sequences are discussed, and it is shown that multi-thruster operation and control is as simple as for a single thruster. Some system architectures require operation of multiple cathodes while they are electrically connected together. Four different methods to control the discharge current emitted by individual cathodes in this configuration are investigated, with cathode flow rate control appearing to be advantageous. Dual-parallel thruster operation with equal cathode current sharing at total powers up to 10 kW is presented.

I. Introduction

The key motivation for the development of direct-drive systems is the desire to significantly reduce the mass of high-power, solar electric propulsion (SEP) vehicles by eliminating most of the heavy, expensive power conditioning electronics between the solar array and the electric thrusters. Although serious investigations were performed in the mid-1970's for ion thruster systems, interest waned with the realization that solar arrays operating at the voltages required by ion thrusters would not be available anytime soon. That interest was rekindled with the availability in the West of Hall thrusters, which require much lower operating voltages, in the 1990's. Although initial direct-drive testing with Hall thrusters demonstrated the feasibility of the concept, the results also raised new questions.[1] A subsequent NASA program was begun to develop direct-drive systems, including an investigation of systems engineering and spacecraft integration,[2, 3] which also identified a number of issues that would need to be resolved before direct drive could be implemented. This work also stimulated other studies of direct-drive systems,[4, 5] but only one other test of a Hall thruster using a solar array.[6]

With an eye toward new high-power applications of solar electric propulsion,[7, 8] NASA made the decision in 2011 to implement a National Direct-Drive Testbed to address the technical issues identified in previous direct-drive investigations. The first results from the Testbed were extremely positive, retiring or significantly reducing nearly all of the technical risks associated with single-thruster operation that were identified prior to the testing.[9] Operation and control of a Hall thruster using direct drive was shown to be simple and the same as with conventional supplies,

* Senior Engineer, Electric Propulsion Group, Senior Member AIAA.
† Principal Engineer, Propulsion, Thermal, & Materials Engineering Section, Associate Fellow AIAA.

with no anomalous power system behavior or oscillations, and easily described with simple photovoltaic and time-dependent electric circuit models. On the strength of these results, direct-drive has been established as firmly within the trade space for new aggressive missions such as the Asteroid Retrieval Mission study.[10]

The Direct-Drive Testbed has recently been used to examine systems-level areas of interest. One of those areas is the use of a Hall thruster as a peak power tracker, which would enable the electric propulsion system to extract the maximum available power from the solar array. Another area of great interest is multi-thruster use in a direct-drive system. Electric propulsion system-level trades suggest that the use of a few to several thrusters is more advantageous for processing large amounts of power than using a single monolithic thruster.[11] This opens up questions regarding operation and control of multiple thrusters, and also questions regarding EP and power system architectures. These issues are the topic of the present investigation.

A. Peak Power Tracking

Peak power tracking is simply the management of loads on a power system to extract the maximum power available from a solar array. In graphical terms, it is the operation of a system at the peak power point of the solar array power-voltage (P-V) curve, an example of which is shown in Fig. 1. NASA robotic spacecraft do not typically employ any sort of peak power tracking feature, but rather design a power system for operation near the peak power at voltages slightly lower than the voltage at peak power (i.e. the left-hand side of the P-V curve).[12] This method does not utilize the full capacity of the array, but for the typical low powers required it is not a major source of concern. As spacecraft grow to higher electrical powers with the addition of SEP systems, however, the added cost and mass of unused array capacity becomes more significant.

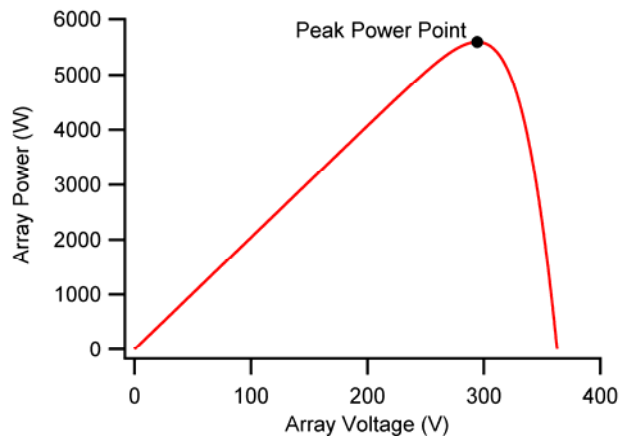

Fig. 1. Sample Solar Array Power-Voltage Curve.

The development and operation of the Dawn spacecraft, on NASA's first science mission to utilize SEP, has shown that knowledge and use of the array power is tightly coupled to mission planning. The use of all available electrical power enables greater thrust and specific impulse from the SEP system, which produces greater margins for completion of trajectories, longer stay times at targets, and greater overall system robustness. The flight operations team needs to be able to predict solar array power with high accuracy throughout the mission to complete its objectives under multiple constraints.[12, 13]

The Dawn spacecraft does not employ a peak power tracker, so the power system is carefully managed to provide as much power to the SEP system as possible while also providing power to the spacecraft bus and holding appropriate power margins in place to maintain power system stability.[14] Unfortunately, the telemetry from the solar array is limited so it is very difficult for operators to know how much power is available to the spacecraft at any given time. Partly for this reason, a complicated off-pointing test was performed early in the mission for in-flight calibration of the power performance models.[12] Greater uncertainty in available array power requires greater power margins for power system stability, hence reduced power available for SEP, which makes it more difficult for flight operations teams to complete their objectives. This result is not limited to Dawn, in general any SEP mission with limited knowledge of array power would face the same hurdles.

An SEP system that could operate with, or as, a peak power tracker would thus provide tangible benefits for NASA spacecraft. A direct-drive Hall thruster system is almost perfectly tailored to fill this role. The thruster itself is a constant current load, which makes operation of the power and propulsion system across the solar array P-V curve extremely simple and robust.[9] If the solar array and power system are designed for separate array segments for the SEP and bus power loads, then issues of power system stability that were a concern for the Dawn system are significantly mitigated. Finally, the Hall thruster system already contains all the necessary hardware to perform peak power tracking functions and no additional hardware would be required to implement full peak power tracking functionality. This paper will discuss the development and design of a peak power tracker that utilizes existing system hardware combined with a newly-developed software control algorithm, and present results from ground-based system testing.

B. Multi-Thruster Systems

One of the major outstanding questions for multiple-thruster operation on high-power spacecraft is that of the architecture of the power and propulsion systems. Multi-thruster systems have been ground-tested extensively and even implemented on flight spacecraft. The present-day implementation of multi-thruster operation on near-Earth spacecraft is similar to that of individual thruster operation, namely a regulated power bus provides power to electrically-isolated thruster-PPU strings. On a direct-drive spacecraft, however, architects have the option to provide power in new and different ways.

First, individual isolated solar array segments could be dedicated to each thruster string. Electrically this would be equivalent to having individual isolated PPUs for each thruster. This architecture would have the advantage of being similar to architectures already flown in space and having a wealth of ground-based test experience. A disadvantage of this architecture would be that either power cross-strapping or a spare array segment would be required to provide fault tolerance. For example, in a system with two 5 kW thruster strings required to complete a mission and a third thruster string required for fault-tolerance, the spacecraft would have to have three 5 kW array segments dedicated to EP use, only two of which could be used at a time. The extra cost and mass associated with the unused spare array segment could be mitigated with power cross-strapping, but that would add system complexity and introduce additional fault modes by itself.

Second, a single solar array segment could provide power to all thrusters in a parallel electric configuration. In this configuration the anodes of each thruster are electrically connected to the positive side of the array, and the cathode(s) to the negative side of the array. An advantage of this architecture is that is does not require spare array segments or power cross-strapping as does the first option. Use of this system configuration opens up other architecture options related to cathodes, specifically the use of one single cathode to provide current to multiple Hall thrusters, a system with fewer cathodes than thrusters, or the use of one cathode per thruster. In the latter cases, multiple cathodes are required to emit current in a parallel configuration where they are electrically connected together.

Shared-cathode operation has been suggested and investigated for both ion thruster and Hall thruster systems. Neutralization tests performed with the mercury ion thrusters on the SERT II spacecraft first suggested that multiple thruster strings in space might be neutralized with the emission current from a single cathode.[15] Researchers at TsNIIMASH have demonstrated single-cathode and parallel-cathode Hall thruster clusters.[16, 17] The U.S. Air Force initiated a program in the early 2000's to investigate the operation of clusters of Hall thrusters,[18] with a focus particularly on cathode and plume effects.

Clusters of Hall thrusters are easily operable from a single cathode, whether they are operated from a single power supply[17] or from individual power supplies for each thruster.[19, 20] Experiments with a trio of D-55 thrusters showed that the thrust produced by the cluster was equivalent to the sum of individual thrusts and that the current oscillations of the thrusters were independent.[17] The distance between the shared cathode and each thruster may have a significant effect on cluster performance[20] although some experiments have suggested this is not an issue.[17, 19] Beal *et al.* concluded that many anticipated advantages in shared-cathode architectures were not realized, specifically with regard to understanding and predicting performance and plume properties.[20, 21]

Operation of multiple ion thruster neutralizer cathodes that were tied together electrically was investigated as a part of the ETS-VI flight mission. Life testing of the ion thrusters for this mission was performed with individual thruster power supplies but with the neutralizers of multiple engines connected electrically through the facility ground.[22] An imbalance of current emitted from each neutralizer in this configuration was observed, and it was demonstrated that this imbalance could be adjusted by changes to the neutralizer mass flow rate.[22, 23] The neutralizers were also tied together electrically on the spacecraft, where current emission imbalance was observed during simultaneous flight operation of two thrusters. Proper adjustment of neutralizer mass flow rate was shown to cause both neutralizers to emit nearly the same current.[24]

Operation of multiple Hall thrusters with their cathodes tied together electrically has not been investigated as thoroughly. This configuration was proposed and demonstrated for a D-55 cluster[16] (no data were reported in the reference). In another test, two BHT-200 thrusters were operated with independent discharge supplies and with the cathodes connected electrically to ground. Under the nominal test conditions one of the two cathodes drew approximately 90% of the total discharge current.[25] Finally, and most relevant for the work described here, Beal *et al.*[20] operated two BHT-200 thrusters in parallel from a single discharge power supply with the cathodes operating at identical mass flow rates and keeper currents. In the configuration of this test, essentially all of the current was emitted from one of the two cathodes.

For application to direct-drive systems, it appears then that multiple architectures may be technically feasible although they have different implications at the system level. Individual solar array segments have the greatest

similarity to the power architecture of conventional flight systems, but there are impacts to cost, mass, system-level complexity, and fault-tolerance. Multiple thrusters can be operated from a single shared cathode, although it appears further work must be done to determine the effects of relative distance between cathode and thrusters on system performance. This would also necessitate the development and qualification of a long-life, high-current cathode for such a system. An additional cathode or cathodes would have to be added to the system for fault-tolerance. Finally, a configuration with multiple cathodes connected electrically together may be attractive if a simple reliable means to control the emission current from each individual cathode can be demonstrated. It has been suggested that this might be possible with additional PPU circuitry, and it has been demonstrated via propellant flow rate control. A major portion of the work described in this paper addresses the means of controlling emission current from cathodes configured in this manner.

II. Experiments in Peak Power Tracking

Many different methods have been employed in terrestrial power systems for peak power tracking.[26] Two of the major methods are readily applicable to Hall thruster operation: the perturb-and-observe method (sometimes called the hill climbing method) and the incremental conductance (IC) method. The perturb-and-observe method is very simple and easy to implement. In a typical terrestrial application, a system controller simply effects a small change in the array voltage and monitors the response of the current supplied by the array. If the power increased, the array voltage change was headed toward the peak power point; alternatively if the power decreased the array voltage change was headed away from the peak power point. Continual application of this strategy ultimately leads to operation at the peak power point. Major advantages of the method include simplicity and ease of implementation. Major disadvantages of this method include continual dithering about the peak power point; lack of knowledge of the location of the operating point on the power-voltage curve, and thus what adjustments are necessary to reach the peak power point; and possible tracking in the wrong direction under rapidly changing irradiance conditions.[27] While the latter issue is not applicable for unshadowed space-based operation, it can be important for terrestrial testing of direct-drive systems.

The perturb-and-observe method can be used with a direct-drive Hall thruster system but the implementation is different because a Hall thruster is a constant-current device, as opposed to the use of a voltage controller in a terrestrial array power system. The method can be easily implemented through changes in the propellant flow rate which changes the operating current, voltage, and power of the thruster (higher flow rates yield higher discharge currents, which moves the system along the array current-voltage curve toward lower voltages). But this method suffers from an additional concern in that there can be a significant lag time between the commanded change in flow rate and the equilibration of the thruster at a new current-voltage operating point because of the propellant tubing line lengths and gas dynamic timescales. Continual changing of the propellant flow rate and waiting for equilibrium can also be wasteful of propellant and could have trajectory implications because of thruster performance changes. These concerns can be mitigated by using the incremental conductance method.

The incremental conductance (IC) method is based on the observation that at the peak power point the slope of the power-voltage curve is zero:[26]

$$\frac{dP}{dV} = \frac{d(IV)}{dV} = I + V\frac{dI}{dV} = 0 \tag{1}$$

Rewriting this equation it becomes:

$$\frac{I}{V} + \frac{dI}{dV} = 0 \tag{2}$$

at the peak power point. We recognize that to the right of the peak power point the power-voltage slope is negative, therefore:

$$\frac{I}{V} + \frac{dI}{dV} < 0 \quad \text{for } V > V_{mp} \tag{3}$$

And to the left side we have:

$$\frac{I}{V} + \frac{dI}{dV} > 0 \quad \text{for } V<V_{mp} \tag{4}$$

In general, then, we can define the IC Parameter as:

$$IC\ Parameter = \frac{I}{V} + \frac{dI}{dV} \tag{5}$$

which will have a zero value at the peak power point and a non-zero value at all other points. Measurement of the current and voltage along with the slope in the current-voltage (I-V) curve can thus tell us if the system is operating at the peak power point, and if not what side of the peak power point it is on and relatively how far away from it the system is. This is shown graphically in Fig. 3**,** where it can be seen that each location on the P-V curve is uniquely associated with a single value of the IC Parameter. The IC method can be a much more efficient and fast way to track the array peak power than the perturb-and-observe method because of the predictive capability, as will be shown. Disadvantages include the increase in computational requirements and difficulties in determining the I-V curve slope because of the noise in real systems.

C. Peak Power Tracking Algorithm Development

Array P-V curves like that shown in Fig. 3 will vary during a mission due to factors such as the heliocentric distance, temperature, array angle feathering, power consumption, and cumulative radiation dose.[28] For terrestrial testing, the time of day, temperature, and atmospheric variations are the largest causes of P-V curve change. As the P-V curves change, so too will the associated IC Parameter curves as shown in Fig. 2. Although this discussion will utilize the terrestrial-based curves, a similar set of curves can be generated for application in space and those will be shown later.

Inspection of the P-V and IC Parameter curves in Fig. 3 and Fig. 2 leads to an important realization. Since each value of the IC Parameter is uniquely correlated to a single location on the array P-V curve, and thus also the I-V curve, there must be an analogous unique correlation between the IC parameter and the anode mass flow rate because of the linear dependence between anode mass flow rate and discharge current of a Hall thruster. With this knowledge a change of variables can be used to generate the curves shown in Fig. 6, which assume a relationship between flow rate and discharge current taken from H6 Hall thruster test data. Note here that for each individual curve (e.g. 13:00) the mass flow rate at the peak power point is determined by where the IC Parameter is equal to zero. If the IC Parameter of a system not operating at the peak power point is known, then, the mass flow change required to arrive at the peak power point can be determined. For example, if a system is operating at 13:00 and the IC parameter is determined to be -0.2, the curve in Fig. 6 shows that an additional 3.9 mg/sec of anode mass flow must be added to reach the peak power point. This works for all IC Parameters values except those sufficiently larger than zero, where there is a non-unique correlation between flow rate and IC Parameter. This region is to the left of the peak power point on the P-V curve, where a direct-drive system can enter the low-voltage operating mode.[9] Fortunately this region is not desirable for spacecraft application.

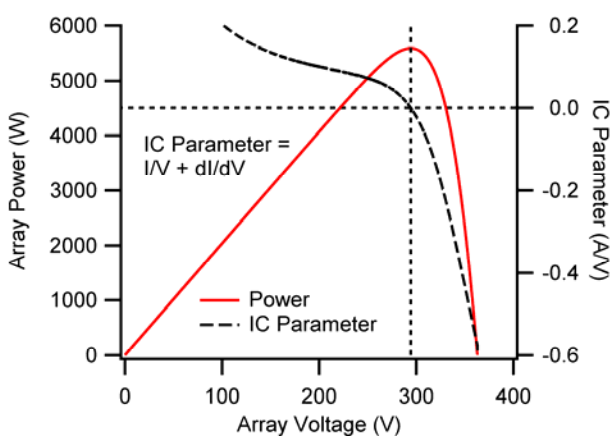

Fig. 3. Sample Power-Voltage Curve with IC Parameter.

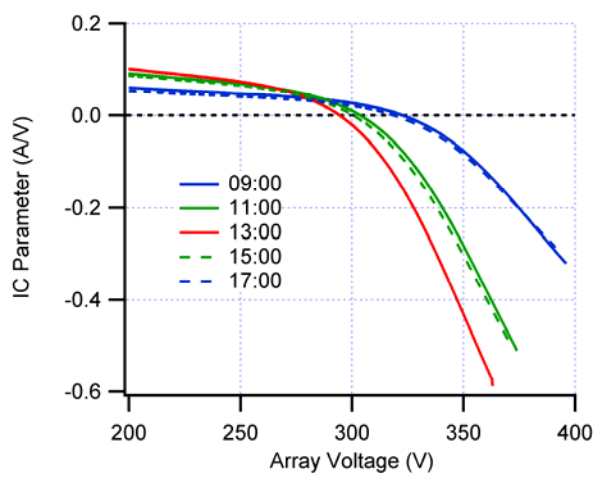

Fig. 2. Sample IC Parameter Curves for Terrestrial Testing at Different Times of Day.

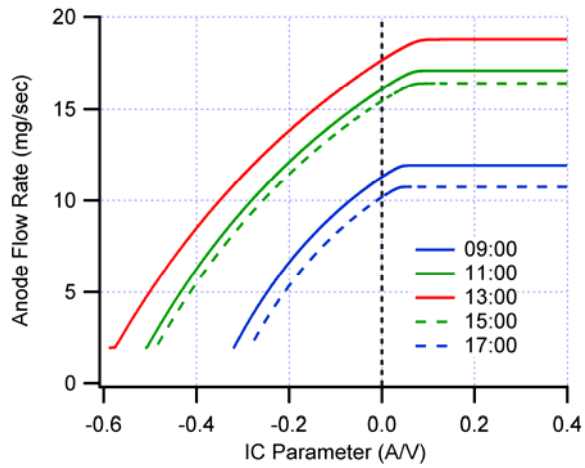

Fig. 6. Dependence of IC Parameter Curves on Time and Flow Rate for the H6.

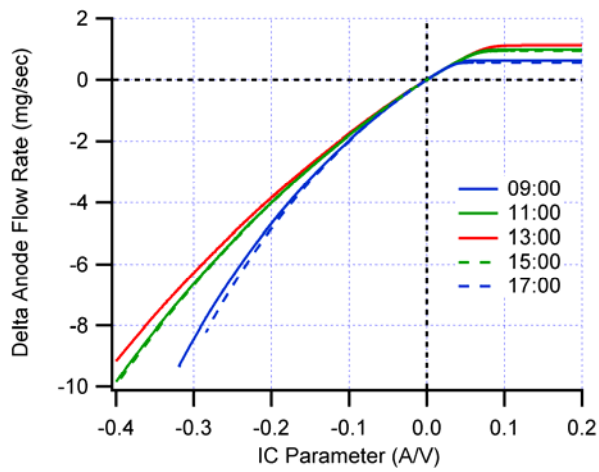

Fig. 4. Collapsed IC Parameter Curves. These curves show the anode mass flow rate change necessary to reach the peak power point for a given IC Parameter.

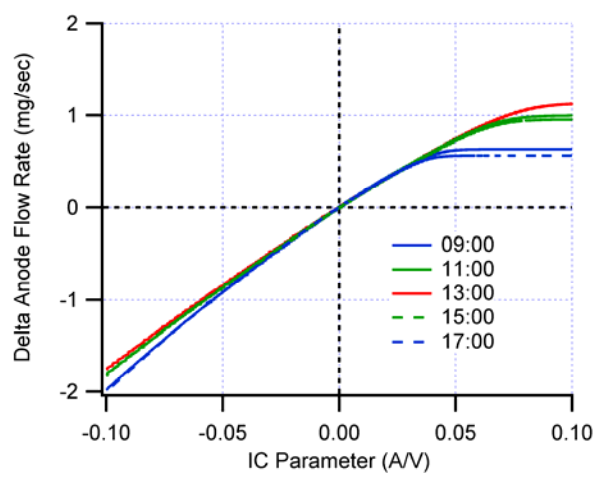

Fig. 5. Collapsed IC Parameter Curves near the Peak Power Point.

The curves shown in Fig. 6 are useful, but in general the P-V curve of a solar array is not known beforehand which complicates the implementation. This can be overcome by collapsing the curves at the peak power point, i.e. re-forming them in terms of the mass flow rate difference from that at the peak power point (IC Parameter equal to zero). This is shown for the full range of interest of the P-V curve in Fig. 4, and for a smaller region near the peak power point in Fig. 5. Note that the curves are very similar to each other over a wide range of conditions, and most importantly are nearly identical and close to linear near the peak power point. Thus, near the peak power point, a single linear relationship can be used to determine the mass flow rate adjustment necessary to reach the peak power point over a wide range of solar array performance curves. This holds true over a range of about 1.5 mg/sec for the curves shown in Fig. 5, which corresponds to a voltage range of about ±11 V about the peak power point for the 1300 hour curve, and +22/-34 V for the 17:00 curve. This is a fairly broad range and is an important result. Further from the peak power point where the IC Parameter has values less than -0.1 the curves diverge. Here the single linear relationship can be still used, however, in combination with a control algorithm that only steps partway toward the peak power point at a single time.

Implementation of the IC method through the IC Parameter (Eq. 5) relies on accurate determination of the slope of the solar array I-V curve at the point of system operation. One way of finding this slope using an existing Hall thruster system is by slightly perturbing the operating point, thus moving to a new location on the array I-V curve. This can be accomplished by a small adjustment in the flow rate, but as mentioned earlier there is a lag time associated with system response and wasted propellant could be a concern. Another method is found by recognizing that changes in the thruster magnet current can be used to make fast, minor perturbations of the thruster discharge current. Proper choice of these magnet perturbations can yield very accurate calculations of the I-V slope. Current and voltage perturbations can be very small and of short duration, such that they do not appreciably affect the performance of the thruster, and they are also nearly instantaneous upon command. An example of such I-V perturbations measured during direct-drive operation of the H6 Hall thruster is shown in Fig. 7. It can be seen that the response is immediate, the duration is short (10 to 15 seconds), and that the discharge perturbations are well defined. For either a laboratory test or for flight, software must be developed to effect the change and measure the current and voltage steps autonomously. A disadvantage of this method is that the slope calculations can be affected by noise in real systems, such as that observed in the figure. Note that minor atmospheric disturbances in ground-

based testing cause the discharge voltage to fluctuate with the constant-current thruster load, and this can also lead to complications in perturbation calculations.

For the laboratory testing described herein, a simple and basic set of instructions was written within the Labview program used at JPL for direct-drive Hall thruster operation. The software was designed to regularly perturb the system operating point through the magnet current and determine the instantaneous value of the IC Parameter, then determine the amount of flow rate adjustment necessary to reach the peak power point using a linear relationship developed from Fig. 5. It also includes rules for magnet current setpoints based on discharge power and limited fault protection. A flow chart of the overall operation is shown in Fig. 8. In practice there is an allowable deadband around the peak power point within which control is not performed. This is indicated in the figure by the comparison of the IC Parameter to a fixed value ε, which could in general be different for positive and negative values of the IC Parameter. Furthermore, it should be noted that this method could be used to control system operation within any set range on an array P-V curve, not just at the peak power. The voltage, current, and power deadband about the peak power point can easily be determined from the values of ε by inspection of the system I-V curve, for example Fig. 3.

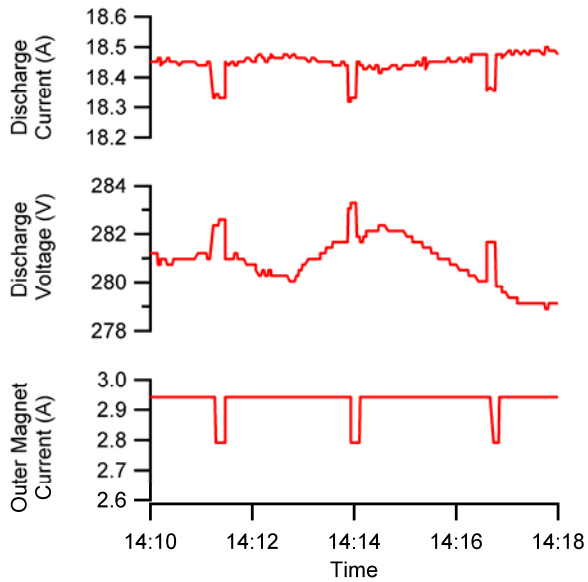

Fig. 7. System Discharge Current and Voltage Perturbations Produced by Commanded Magnet Current Perturbations.

D. Experimental Setup

Peak power tracking experiments were performed with the National Direct-Drive Testbed. The Testbed consists of a set of fifty-six commercially-available terrestrial solar panels and a power control station designed specifically to provide flexibility in solar array electrical configuration. Each 1.60 m × 1.06 m panel includes ninety-six 15%-efficient mono-crystalline silicon solar cells and provides a minimum of 255W under Standard Test Conditions (1000 W/m^2, spectrum AM1.5, 25 °C).[29] Solar irradiance, cell temperature, and solar spectrum affect the actual output in field use. The array as installed can produce a maximum of 12 kW for direct-drive operation under ideal conditions, although for reasonable test durations under typical environmental conditions the maximum useable power is about 10 to 11 kW. Further description of the Testbed, and details on the photovoltaic model used to generate I-V and P-V curves, is presented elsewhere.[9] The photovoltaic model has been upgraded to include the effect of resistive losses in the array wiring and power control station.

The H6 thruster is a 6-kW-nominal laboratory Hall thruster that was developed as a testbed for studies of thruster physics and developments in diagnostics and thruster technology. The thruster was a joint development between JPL, the University of Michigan, and the Air Force Research Laboratory and continues to be studied at those institutes. The throttling range of the thruster is approximately 0.6-12 kW discharge power, 1000-3000 s specific impulse, and 50-500 mN thrust. Over 70% total efficiency is achieved at discharge voltage of 800 V. At the nominal

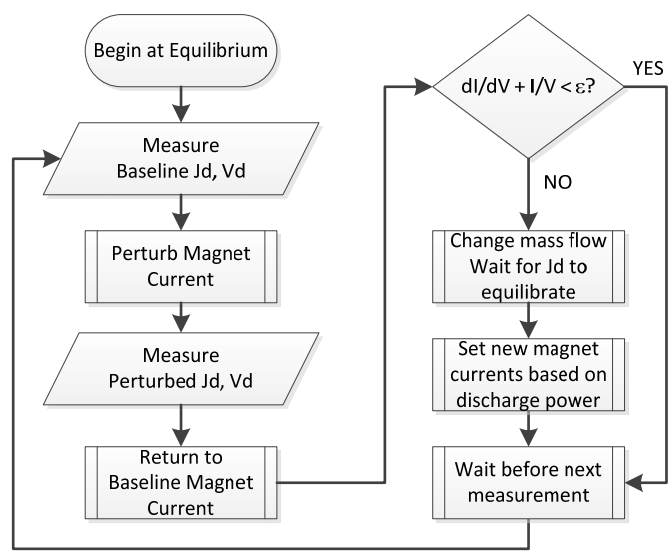

Fig. 8. Control Flow Chart for the Incremental Conductance Method of Peak Power Tracking.

300 V, 6-kW condition, thrust, total specific impulse, and total efficiency are 406 mN, 1970 s, and 65%, respectively. A centrally-mounted lanthanum hexaboride cathode was used for this work with a flow fraction of 7%. Direct-drive operation of the H6 thruster has been studied in detail.[9]

All testing was performed in the Al Owens vacuum test facility at JPL. The vacuum chamber is 3 m in diameter and 8.6 m long, with ten cyropumps installed and operational for this testing. With the vacuum chamber configuration used for this test the effective pumping speed was approximately 200 kL/s on xenon. To minimize facility backsputter rates the interior of the vacuum facility is lined with graphite panels. Xenon flow and electrical power for the thruster ancillary functions were both provided with standard laboratory systems.

The power system, flow system, and facility telemetry were controlled and monitored with a Labview-based data acquisition and control system. The data system recorded thruster currents, voltages, and flow rates as well as facility and solar array data at a user-specified rate, typically several times a minute. The software used to record data was also used to control thruster power supplies and flow rates.

Global hemispherical solar irradiance was measured in real-time with a dedicated instrument located about 200 m south of the solar array installation. Data were logged using a separate data system, also at several times a minute. This instrument was not calibrated prior to testing and was used for indication in combination with a photovoltaic performance model.

E. Experimental Results

Preliminary testing of the peak power tracking control algorithm (hereafter referred to as the peak power tracker, or PPT) was performed in a short series of multi-hour tests where the PPT was engaged prior to solar noon and allowed to operate as the sun moved across the sky (conveniently simulating heliocentric in-bound and out-bound trajectories). The results of a 4.7-hour-long test are shown in Fig. 9, where the thruster discharge power provided by the solar array is plotted along with the predicted solar array peak power. Solar irradiance increased from 880 W/m^2 at the beginning of this test to 1030 W/m^2 at solar noon, then decreased to 810 W/m^2 by the end of the test. The available solar array power was calculated using the Testbed photovoltaic model with the measured solar irradiance and environmental temperature; in a calibration check performed prior to this test the PV model overpredicted the measured peak power by 3.5% at a single time of day, so this curve should be considered to be not exact but a close approximation of what the peak power is expected to be.

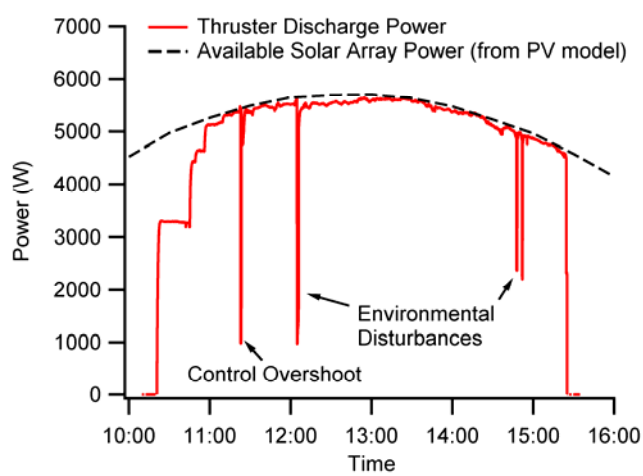

Fig. 9. Direct-Drive Peak Power Tracking Demonstration.

In this test the H6 thruster was ignited at 3.3 kW and operated for about twenty minutes before the PPT was engaged at 10:45, two hours and fifteen minutes before local solar noon. The PPT began by perturbing the magnet current as discussed previously to determine the slope of the array I-V curve and then the IC parameter. Various safety limits in the control algorithm limited how quickly flow rate changes could be made and how large they could be. Shortly after PPT engagement the thruster discharge power was within ~2.5% of the predicted array peak power and within the PPT controller deadband. The PPT tracked the predicted array peak power well from the time it was engaged, even operating at almost exactly the peak power at many times, until it was turned off 2.5 hours after solar noon.

The control system deadband for this test was set at IC Parameter values of -0.05 to +0.01. The effective deadbands in system current, voltage, and power depend on the instantaneous values of the array I-V curve which change as a function of time in terrestrial test. Taking for example the I-V curve of Fig. 3 which is similar to the I-V curve predicted on solar noon of this test day, the total deadband about the peak power point would be a discharge current of 1.05 A, discharge voltage of 15.5 V, and a discharge power of up to 86 W less than the peak power (i.e. 1.5% of the peak power in the figure). The PPT algorithm can easily be changed to encompass a different deadband range at the peak power or away from the peak power if desired.

At four times during this test the system went beyond the peak power point and into a low-voltage mode of operation, seen in the data of Fig. 9 as short but significant drops in discharge power. The first event was traced to calculation of an incorrect IC Parameter most likely resulting from a magnet current change directed by the part of

the control software that maintains appropriate magnet currents based on thruster power level, which occurred during the same time as the PPT was trying to measure the I-V slope. This should not have been allowed and can be corrected through control system software improvements. The second event was caused by a transient atmospheric disturbance, evidenced by the measured solar irradiance which dropped from 1005 W/m^2 to 920 W/m^2 for a period of about thirty seconds at this time. The latter two events were traced to an outgassing event that caused an uncommanded increase in the thruster discharge current (this test was the first thruster operation after it and the facility had been exposed to atmosphere). The PPT control algorithm detected the change but was unable to compensate for it quickly enough. The limited fault tolerance built into the PPT control algorithm, however, was able to prevent any other excursions.

An example of PPT operation and correction near the peak power point is shown in Fig. 10. The PPT algorithm calculated the IC Parameter at 11:49 and determined that a mass flow increase was necessary to increase the system operating power. The PPT was programmed to monitor the system operating point quickly after a flow system change, so at about ninety seconds later another IC Parameter measurement was performed. Here it was determined that the system had passed through the peak power point outside of the control deadband, hence a mass flow decrease was commanded. At 11:52 another IC Parameter measurement was performed and the PPT determined that the system was now operating within the control deadband so no further mass flow changes were commanded. The system ended up operating at a slightly higher discharge current than before the measurement at 11:49. Post-test data analysis showed that the mass flow increase determined by the PPT at 11:49 was larger than necessary, due to difficulty in calculating the I-V slope from the system telemetry at this time. Further refinements in the PPT control algorithm are expected to improve the accuracy of the IC Parameter calculation and hence PPT execution.

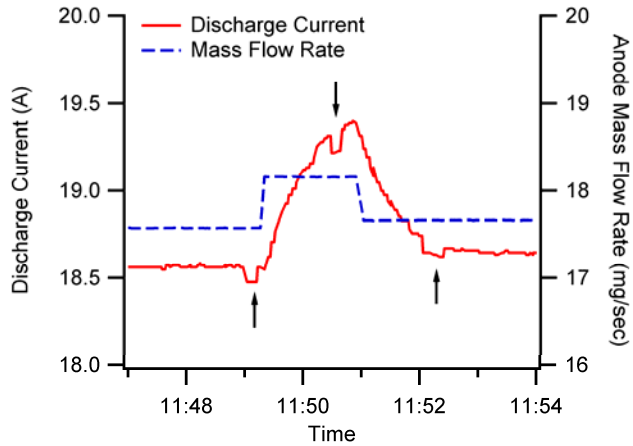

Fig. 10. Peak Power Tracking Control Algorithm Performance Near the Solar Array Peak Power Point. The arrows show discharge current perturbation events used by the controller to determine the IC Parameter.

F. Application to Space Operation

The IC method for peak power tracking is easily transferrable to space-based operation. Array P-V curves for near-Earth operation, shown in Fig. 11, can be used to generate IC Parameter curves for the H6 thruster as shown in Fig. 12. These curves show greater variation for large negative values of the IC Parameter, and a smaller linear region near the peak power point, than do the terrestrial curves. Nonetheless, similar behavior exists thus it is

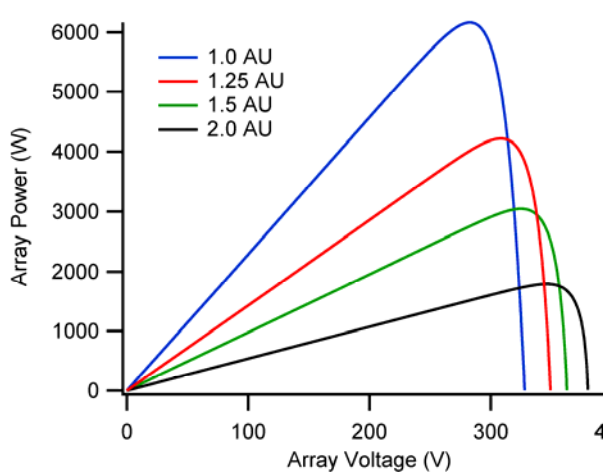

Fig. 11. Sample P-V Curves for Different Heliocentric Distances.

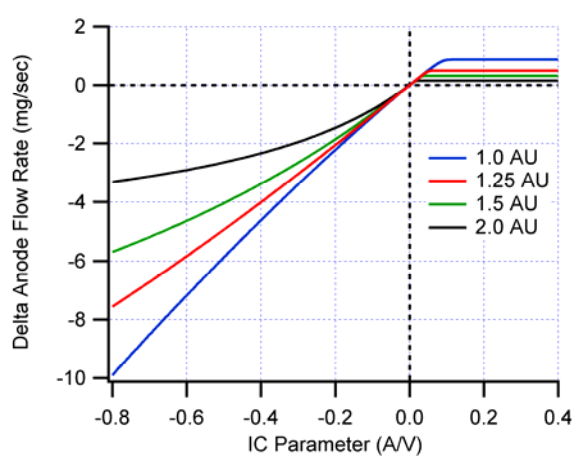

Fig. 12. Collapsed IC Parameter Curves for H6 Thruster Space-Based Operation.

reasonable to expect that a peak power tracker based on the IC method shown here could be developed. Under some combinations of environmental conditions it is possible that P-V curves could change shape near the peak power point (e.g. low intensity, low temperature conditions) so further examination is warranted.

Finally, the IC method has been shown here to be powerfully predictive and versatile. If a spacecraft system is intended to be operated at or near the peak power point for very long durations without change, however, it should be possible to find the peak power point with the perturb-and-observe method and then fix the thruster operating condition for as long as the array performance is relatively constant. This avoids the additional computational complexity of the IC method but sacrifices the additional knowledge and performance that the IC method can provide. If a spacecraft needs to change EP power levels rapidly or frequently, or control the EP power at a point other than the array peak power point, the IC method would be preferred.

III. Experiments in Dual Thruster Operation

Prior to recent investigations at JPL, serious technical questions made it difficult to baseline the use of direct drive in missions for which it could provide great advantages. While single-thruster issues were addressed in the previous study,[9] multi-thruster issues were deferred. The remaining technical issues for dual-thruster operation identified in that study are shown in Table 1, along with two others added more recently. The issues in this table are the focus of the present work.

Table 1. List of Identified Dual-Thruster Direct-Drive Technical Issues.

1	How do you start, stop, and operate multiple Hall thrusters in a direct-drive system?
2	How do you operate near the peak power point with multiple thrusters?
3	What additional filtering is necessary when operating multiple thrusters in parallel?
4	Is current sharing possible with all of the cathodes tied together?
5	How do you enforce cathode current sharing for multiple Hall thrusters in a direct-drive system?

A. Experimental Setup

Dual-thruster testing was performed in the same vacuum facility using the same support equipment as described earlier (Section IID). Instead of the H6 thruster, however, this testing used two versions of the NASA-173M Hall thruster, version 2 and version 3 (hereafter referred to as v2 and v3). The NASA-173M was developed to examine high-specific-impulse operation and is sized to operate at a nominal 10 A of discharge current with discharge voltages of 500 to 800 V. The 173M v2 has been characterized at a much wider range: discharge currents of 4 to 16 A and discharge voltages of 300 to 1000 V, over which it produces 80 to 440 mN of thrust at efficiencies of 48 to 64%.[30] Following that work a v3 thruster was designed and fabricated with only minor mechanical changes; no changes were made to the discharge chamber geometry, wall material, anode design, or magnetics.[31] The first operation of the v3 thruster was as a part of the direct-drive work described here.

A pair of laboratory barium-oxide cathodes were paired with the thrusters for the initial proof-of-concept testing. The cathode geometries were similar; the cathode paired with the v2 thruster had an NSTAR-like design,[32] whereas the v3 cathode had a slightly larger cathode orifice diameter and a deeper chamfer. Results from the initial dual-thruster testing demonstrated that cathode operation had a significant effect on cathode current sharing, so in subsequent testing these laboratory cathodes were replaced with identical flight-spare discharge cathodes from the Dawn project.[33]

The thrusters were installed in the vacuum facility with coplanar exit planes and parallel centerlines separated by 36 cm (slightly more than two thruster discharge chamber diameters). Each laboratory cathode keeper face was located 21 mm downstream of the thruster exit plane and its centerline was 27 mm from the outer edge of the thruster; the flight-spare cathodes were located slightly further downstream at 25 mm from the thruster exit plane. A photograph of the installation is shown in Fig. 13.

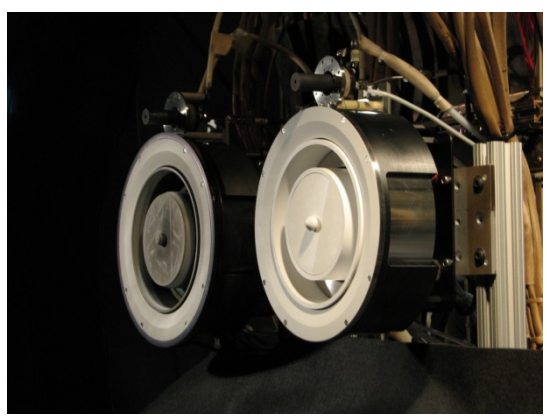

Fig. 13. NASA-173M v2 (left) and v3 (right) in Dual-Thruster Test Configuration with Laboratory Cathodes.

A simplified electrical circuit schematic for the dual-thruster test is shown in Fig. 14. The thrusters were connected directly to the discharge power source with an intervening 80 μF electrolytic filter capacitor. Both solar and conventional power supplies were used to drive the thruster during testing and the configuration was easily switched between the two. The output of the different combinations of solar panels coming from the array power control station is represented in the figure by a single circuit element. The figure does not show the several safety disconnect switches associated with the solar system, nor the cathode clamping circuit used to keep the negative side of the circuit from wandering too far from ground. Also not shown are the conventional cathode heater, cathode keeper, and magnet power supplies that were isolated from the discharge power circuit and from each other. The thruster anodes were tied together inside the vacuum tank. Each cathode return line was separately brought outside of the vacuum tank and connected to a separate, selectable ballast resistance. The ballast resistors used for the initial proof-of-concept testing with the laboratory cathodes were 0.9 Ω total with increments of 0.23 Ω, and for subsequent testing with the flight-spare cathodes the resistors were 0.5 Ω total with increments of 0.01 Ω. Total wiring and connector resistance in the cathode lines from the ballast resistor to the cathode flying leads was measured with a micro-ohmmeter and was 35.6 mΩ for the v2 leg and 95.0 mΩ for the v3 leg.

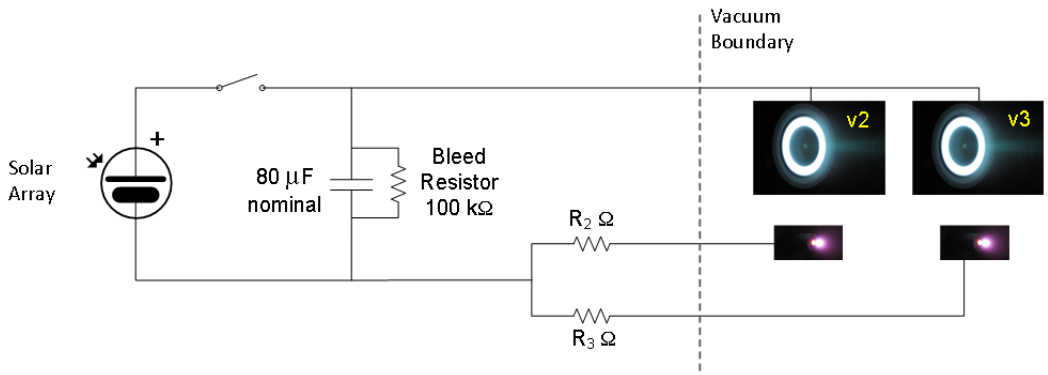

Fig. 14. Simplified Electrical Schematic for Dual-Thruster Testing.

B. Experimental Results

1. Operation and Control

Startup of the second thruster in a dual-parallel configuration is relatively simple and similar to startup of a single thruster. For single thruster startup using direct drive, a softstart method was developed where the cathode was ignited first, then solar array voltage applied to the anode, and finally anode flow initiated. This limited the inrush current during discharge ignition and minimized thruster and power system transients.[9] In the dual-thruster configuration used for these experiments, voltage was already applied to the non-operating thruster when the other thruster was running. With the first cathode and thruster running, the first step in ignition of the second thruster was to ignite the second cathode. At the moment of ignition the two cathodes began to share the discharge current for the first thruster. Next, with the magnet current established and the voltage already applied to the anode, xenon flow was initiated to the second thruster. As for single thruster ignition, the xenon pressure in the second thruster discharge chamber slowly increased to the point at which breakdown occurred and the discharge was established. Either thruster could be shutdown simply by removal of anode flow as demonstrated for single-thruster operation.

Examples of thruster startup and shutdown in the dual-parallel thruster configuration are shown in Fig. 16. The v2 thruster was operating at a steady 340 V, 10 A discharge using the solar arrays near solar noon. As soon as anode flow was initiated to the v3 thruster the total solar array current increased quickly from 10 A to 19 A and the array voltage decreased, following its I-V curve, to 320 V. Total system power increased accordingly. No macroscopic transients in the v2 thruster or power system were observed as the v3 thruster was started (shorter-duration transients have not yet been investigated using an oscilloscope). The v3 thruster was then shut down by removing anode flow, again without observation of macroscopic transients. Another v3 start is also shown in the figure. Throughout this study, repeated startups and shutdowns of thruster were successfully performed using this method without issue.

Control of multiple operating thrusters on the solar array I-V curve was accomplished through anode flow adjustment and the associated magnet current adjustment for thruster power level. In this there was no difference from operating a single thruster. An extreme case is shown in Fig. 15 where the two thrusters were rapidly throttled

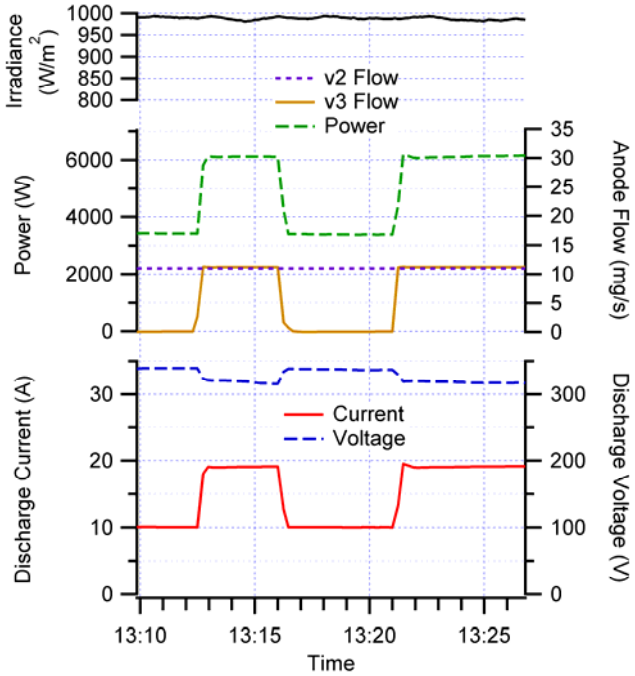

Fig. 16. Dual Thruster Startup and Shutdown.

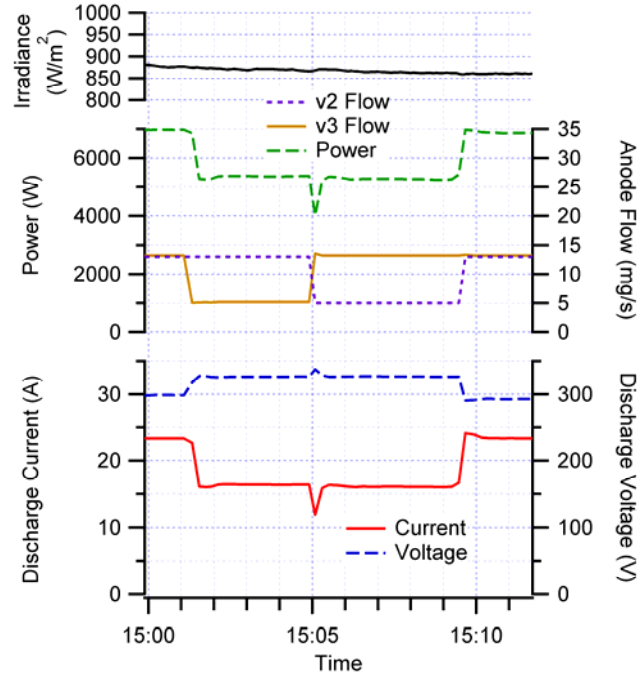

Fig. 15. Rapid Simultaneous Throttling of Dual Thrusters.

in opposite directions of power. Both thrusters were operating at 13 mg/sec of anode flow for a total of 23 A of current and 7 kW of power from the solar array, which was about 85% of the array peak power at this time. The v3 thruster was throttled down to 5 mg/sec while the v2 thruster remained at 13 mg/sec, for a total of 16.4 A and 5.4 kW from the array. Then, the v2 flow was throttled down from 13 to 5 mg/sec at the same time that the v3 flow was throttled up from 5 to 13 mg/sec. A slight dip in the total array current is observed as flow rates equilibrated in the long tubing lengths between the mass flow controllers and the thrusters, but otherwise the rapid throttling of the system was uneventful. Finally, the v2 thruster was brought back to its original operating condition for a total system power of 7 kW. No issues were observed during this investigation regarding throttling of thrusters individually or together.

Dual thruster operation near the solar array peak power point is shown in Fig. 17. Here, the flow rates for each thruster were increased in tandem while approaching and passing through the peak power point (note in the figure that the array power decreased as flow was increased, indicating that the system was operating at voltages lower than the peak power voltage). As for single-thruster operation,[9] at some point past the peak power the system went into a low-voltage mode of operation. The v2 flow rate was then reduced to bring the system out of low-voltage mode, again in the same manner as for single-thruster operation. The v2 flow rate was increased to drive the system into low-voltage mode again, after which it was held constant and the v3 flow rate was decreased to recover from low-voltage operation. System behavior during this process was the same as for single-thruster operation.

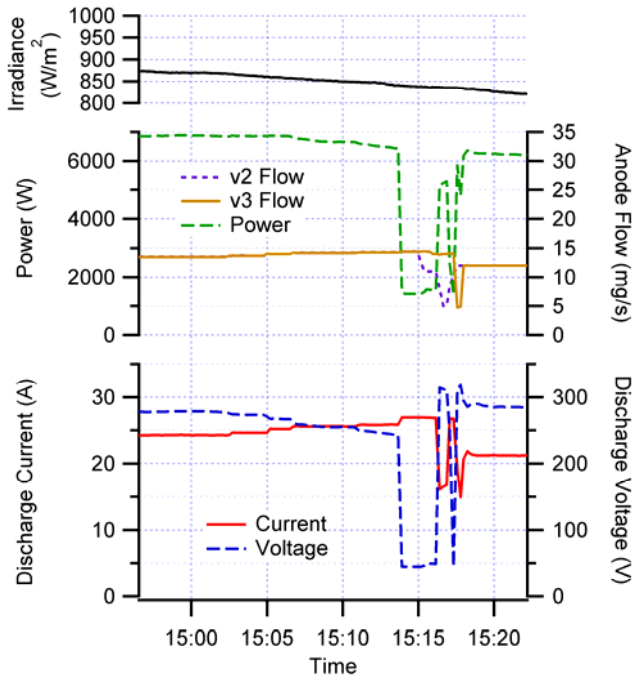

Fig. 17. Dual Thruster Operation Near the Array Peak Power.

In summary, operation and control of a dual-parallel thruster configuration using a direct-drive power system is essentially the same as for a single-thruster system. The softstart method can be used to start the second thruster, and either thruster can be throttled easily across the solar array I-V curve using the anode flow rates. At the system level, total flow rate is the parameter that drives operation on the I-V curve independent of the number of thrusters used. This is expected to hold true for an arbitrary number of thrusters based on the results of this investigation.

2. Cathode Current Sharing: Laboratory Cathodes

One major area for investigation in this study was to determine the ability (or lack thereof) of multiple cathodes connected together electrically and operating in parallel to share current equally, and if the amount of current emission in a single cathode could be controlled through means already existing in a conventional Hall thruster system (or could be added with minor impact). Equal current sharing in this context means the ability of each cathode in a multi-cathode system to emit roughly the same fraction of the total discharge current. Four "knobs" were identified as potential means to affect the sharing of current between cathodes: cathode heater current, cathode keeper current, cathode flow rate, and cathode leg ballast resistance (shown in Fig. 14 as R_2 and R_3). The effects of each of these knobs were examined in the first test configuration which consisted of the laboratory cathodes with slightly different geometries and the coarse ballast resistor increments.

The effects of cathode heater current on cathode discharge current sharing are shown in Fig. 18. In this test the total discharge current was 19.2 A with the v3 cathode carrying 6.3 A (33% of the total) at the beginning of the test. As soon as heater current was applied to the v3 cathode it began to emit more of the total discharge current, and after about five minutes the rate of change of discharge current had considerably slowed, though it was not yet in equilibrium. Further increases in v3 heater current brought the cathodes to near equal sharing at 53% / 47% of the total discharge current. When the v3 heater current was next increased from 5.0 to 5.5 A, however, the cathode sharing quickly *reversed* direction and became more unequal. Returning the v3 heater to 5.0 A slowed the effect but did not change its direction. Twenty minutes later the system appeared to be moving toward an equilibrium state with cathode currents more unequal than before the heater current was first applied, but the test was concluded before equilibrium was reached. This non-monotonic and non-linear response to application of heater current was surprising. Because of this and the slow response times, and additionally because of the heater lifetime impacts associated with long-duration operation at higher currents, cathode current sharing control via heater current was not investigated further.

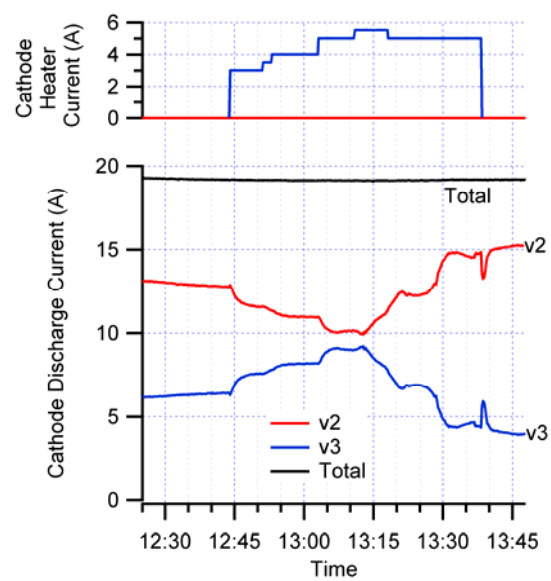

Fig. 18. Effect of Cathode Heater Current on Current Sharing.

The effects of cathode keeper current on cathode discharge current sharing are shown in Fig. 19. In this test the total discharge current was 19.2 A with the v3 cathode carrying 7.5 A (39% of the total) at the beginning of the test. As soon as a small keeper current was applied to the v3 cathode the sharing became more unequal. Application of keeper current to the v2 cathode only increased this trend, which was ultimately reversed by increasing the v3 cathode current to 2.0 A while the v2 keeper current remained at 0.5 A. The system was allowed to equilibrate, where it slowly approached an equal-sharing state before rapidly

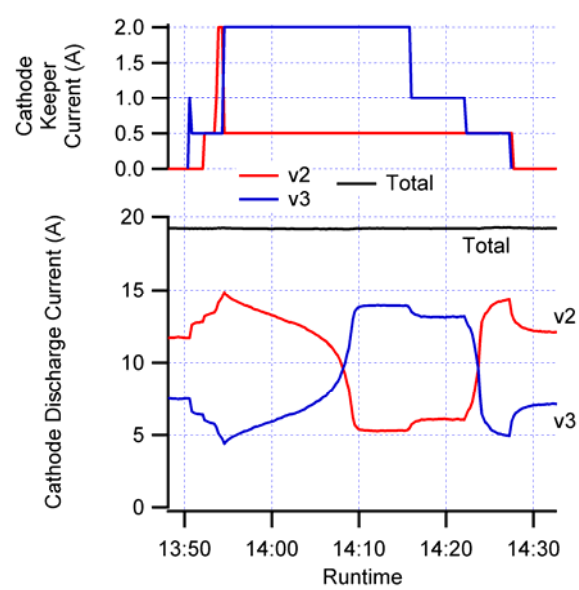

Fig. 19. Effect of Cathode Keeper Current on Current Sharing.

diverging and swapping dominance. After about 17 minutes a new equilibrium was reached where the v3 cathode was carrying 72% of the total current. Subsequent reductions in v3 keeper current cause another dominance swap, then turning off both keepers led to an equilibrium state the same as at the beginning of the test. While it might be possible to find combinations of keeper currents that lead to equal sharing through different combinations of operating conditions or ballast resistance, the long times required for equilibration and the dominance-swapping behavior make this method unattractive.

The effects of cathode flow rate on cathode discharge current sharing are shown in Fig. 20. In this test the total discharge current was 19.6 A with the v3 cathode carrying 4.9 A (25% of the total) at the beginning of the test. Reduction of either cathode flow rate in this case caused the sharing to become more equal, and the combined reduction to a cathode flow rate of 0.75 mg/sec caused the sharing to be nearly equal, 51.2% and 48.8% of the total current, respectively, for the v2 and v3 cathodes. The flow rates were then adjusted in tandem by larger amounts to demonstrate the speed and reproducibility of the effects. Here there is clearly a much better response time compared to the changes in heater current and keeper current; the system response does not show the variable time-rates-of-change and longer equilibration times that were observed for latter control knobs.

Since cathode current sharing control via cathode flow rate control showed promise the effects were studied under a larger range of test conditions. For example, an attempt to cause equal sharing under the test conditions of Fig. 20, but with different flow rates for the v2 and v3 cathodes, had limited success (sharing as good as 45.7% / 54.3%) and demonstrated dominance swapping like that seen in Fig. 19 instead of approaching a state of equal sharing. At reduced power, however, nearly equal sharing was possible with different cathode flow rates. In a test similar to that shown in Fig. 20 but with total cathode leg resistances of 0.94 and 0.79 Ω, sharing was limited to 38.1% / 61.9% with rapid dominance swapping during flow rate changes. Clearly, there is some system interplay between changes in cathode operating conditions, thruster operating conditions, and cathode leg resistance that requires more investigation.

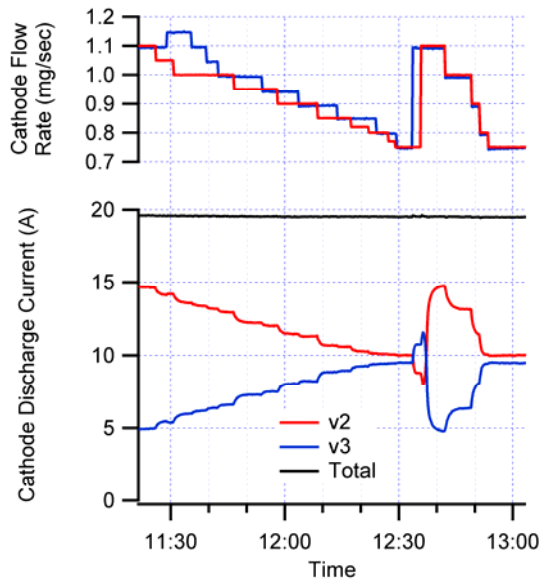

Fig. 20. Effect of Cathode Flow Rate on Current Sharing.

A limited amount of tests were also performed using the same cathode operating conditions but different ballast resistance combinations and, as expected, showed that (1) different ballast resistances caused a different current sharing ratio, and (2) a significant difference between cathode leg resistances caused a large difference in the discharge current sharing between cathodes, even to the point where one cathode was emitting all of the discharge current. These effects were not examined thoroughly in this preliminary test because of the differences in cathode geometries and the coarse increments of ballast resistance that would likely have obscured the dependencies.

Finally, a test was performed to determine if cathode sharing control could be maintained during engine throttling, the results of which are shown in Fig. 21. The v3 cathode and thruster were first lit and operated at a 3.1 kW operating condition. When the v2 cathode was lit at 12:04 it immediately began to draw some of the discharge current from the v3 cathode, and then when the v2 thruster was lit at 12:10 the cathode flows were adjusted in an attempt to control roughly equal sharing during throttling. As the anode and cathode flow rates were regularly increased over a span of 24 minutes from 6.2 to 10.1 kW of

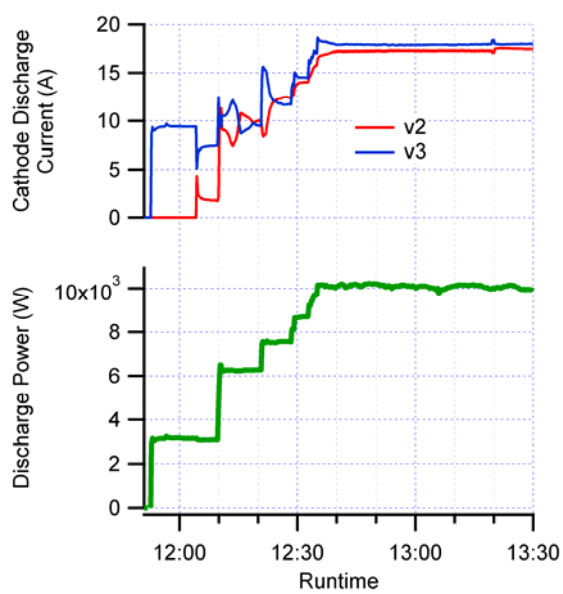

Fig. 21. Operation at 10 kW Total Power with Equal Cathode Current Sharing.

total discharge power, current sharing was controlled using cathode flow rate adjustments. Ultimately the system was operated for an hour with the cathodes sharing discharge current at 49.1% and 50.9%, respectively, on the v2 and v3 cathodes at 10 kW of total system power.

In summary, cathode current sharing in a dual-parallel thruster configuration is possible and is controllable through the use of multiple control "knobs." Equal sharing was not demonstrated with cathode heater and keeper current control in the limited cases investigated, although sharing might be possible under the right combination of operating conditions. Nonetheless, cathode heater and keeper current control are not attractive means because of the non-linear responses and longer durations required for equilibration. During all of these tests with laboratory cathodes, it appeared that differences in laboratory cathode geometry and total cathode leg resistance could have been driving some of the results, so follow-on tests were performed with different hardware to remove these variables.

3. Cathode Current Sharing: Dawn Flight-Spare Cathodes

Only a short amount of time was available for testing with the flight-spare cathodes, so the test goals were limited to characterization of dual-thruster operation with identical cathodes and identical cathode-leg resistances, and identification of the minimum ballast resistance required for cathode sharing. The only control "knobs" investigated for cathode sharing were cathode flow rate and ballast resistance; cathode heater and keeper current were not applied for any of the testing discussed in this section. The results of an initial test performed with a total cathode leg resistance (wiring resistance plus added ballast resistance) of 576 mΩ in each cathode leg are shown in Fig. 22. For this test all controlled thruster operating conditions for both thrusters were identical, including cathode flow rate. The top portion of the figure shows that the two cathodes shared current equally over a range of cathode flow fractions from about 4% to 6%, and outside of this range discharge current emission from the v3 cathode began to dominate. The bottom portion of the figure shows that at equal current sharing the cathode coupling voltages were the same, but they diverged as the sharing became unequal. The v3 cathode, which emitted the bulk of the discharge current at flow fractions greater than 7%, became much less negative than its counterpart as the flow fraction continued to increase. The v2 coupling voltage behavior seen in Fig. 22 is different than when the thruster was operated by itself, where the coupling voltage was much less negative and was similar to the v3 cathode (e.g. -12 V at 9% flow fraction). These initial results suggest that there is some slight uncontrolled difference in the test configuration or hardware that favors emission from the v3 cathode when both thrusters are operated together. Note that the cathode location with respect to the thruster was not optimized, so the coupling voltages were more negative than have been observed in other tests (i.e. -8 to -12 V).[34]

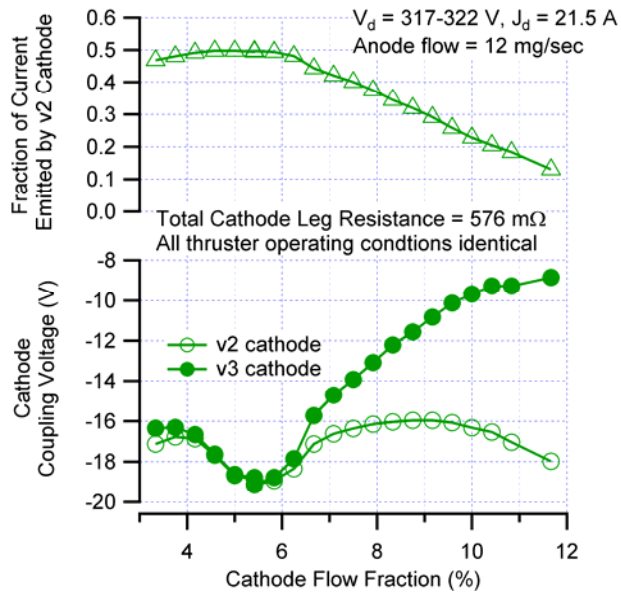

Fig. 22. Cathode Sharing Behavior for Identical Operating Conditions and Cathode Leg Resistances.

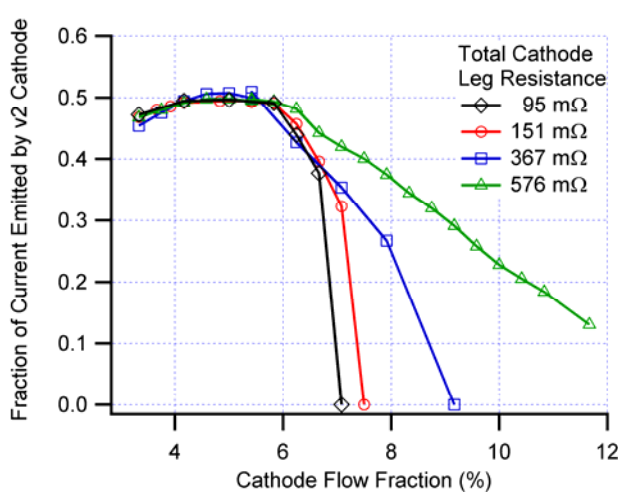

Fig. 23. Cathode Sharing Behavior with Varying Cathode Leg Resistance.

The effects of variation in total cathode leg resistance are shown in Fig. 23 for identical thruster operating conditions. An important result here is the demonstration of equal cathode current sharing with no ballast resistance added to the circuit, only the

95 mΩ of wiring resistance in the cathode legs (note that approximately 60 mΩ of ballast resistance was added to the v2 leg to bring its total resistance to 95 mΩ). This shows that it is possible to operate cathodes equally in parallel Hall thruster discharges without adding ballast resistance and hence system inefficiency to the power circuit. The cathode sharing behavior was the same for each resistance value for flow fractions of 3% to 6%. There is also a clear trend observed at greater flow fractions, in that the dominance of the v3 cathode became more pronounced at lower cathode leg resistances. For example, at an 8% flow fraction the v2 cathode emits a considerable share of the discharge current for resistances of 367 mΩ and 576 mΩ, but at the lower resistances the v2 cathode emits none of the discharge current.

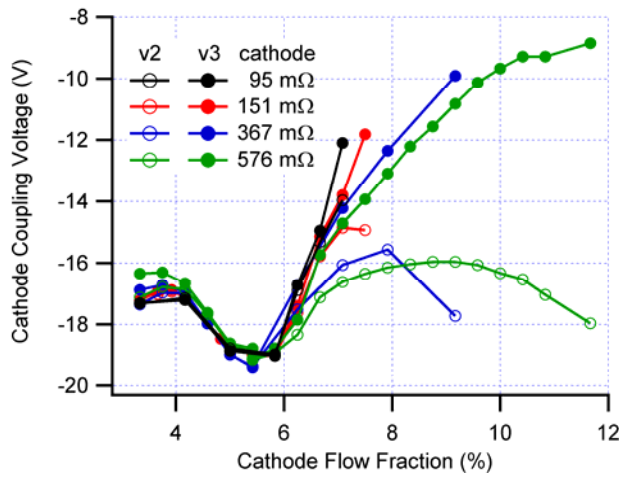

Fig. 24. Cathode Coupling Behavior with Varying Cathode Leg Resistance.

As resistance was changed, the cathode coupling voltage behavior, shown in Fig. 24, was similar to that observed in Fig. 22. Coupling voltages for the two cathodes were equal in the -17 V to -19 V range at flow fractions of 3% to 6%. At greater flow fractions the coupling voltages showed diverging trends as cathode flow was increased, and this occurred at lower flow fractions as the resistance was decreased. Because the coupling voltage at equal sharing did not change as the cathode leg resistance was increased, the net accelerating voltage for the ions must have been decreasing because of the increased voltage drop in the ballast resistance. This is an example of a thrust efficiency loss due to the addition of ballast resistance.

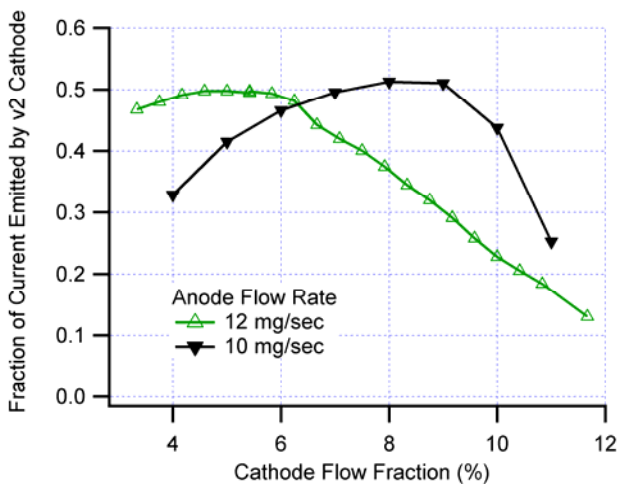

Fig. 25. Cathode Sharing Behavior For Different Anode Flow Rates.

Finally, it is noted that this demonstrated sharing behavior as a function of cathode flow fraction also depends on thruster power level. A single test was performed at the conditions of Fig. 22 but with a lower anode flow rate of 10 mg/sec, and the results are shown in Fig. 25. The cathode flow fraction range for equal cathode current sharing moved from near 5% for the 12 mg/sec anode flow (i.e. 0.6 mg/sec cathode flows) to near 8% for the 10 mg/sec anode flow case (i.e. 0.8 mg/sec cathode flows). The reason for this is unknown as of yet, but it could be an indication that neutral density in the cathode region has an influence on cathode sharing behavior. More work is necessary, and a companion effort has been initiated to gain better understanding of the physics involved in cathode current sharing.[35]

IV. Conclusion

With the significant mitigation or retiring of technical risks associated with single-thruster direct drive operation, attention has moved toward systems-level areas of interest. One of those areas is the use of a Hall thruster system for peak power tracking, which has the potential to extract the maximum possible power out of a solar array and thus provide tangible benefits for mission planning and operations. The perturb-and-observe and incremental conductance methods are both candidates which require no new hardware for a Hall thruster system. While the perturb-and-observe method is simple and could be easily implemented on a flight system, there are many operational disadvantages. The incremental conductance method avoids these issues and provides greater knowledge of system status. An elegant application of this method was developed for Hall thruster systems, whereby small perturbations in the thruster magnet current are utilized to determine the system operating point on

the array power-voltage curve. This knowledge is used to calculate the mass flow rate change required to move the Hall thruster operating point to the array peak power point. A computer algorithm was developed to implement the method and peak power tracking was demonstrated over a 4.7-hour period where the solar irradiance varied by ~20%. The incremental-conductance peak power tracker performed very well while tracking the predicted solar array power available.

Many power and propulsion system architectures exist for a multi-thruster direct drive system, including those in which Hall thrusters are connected electrically in parallel to a single solar array segment. A subset of those architectures includes ones which have individual thruster cathodes that are connected together, electrically in parallel. To investigate the feasibility of these architecture options, a dual-parallel thruster test configuration was created to examine multi-thruster operation and control, and also current sharing between cathodes. A startup process that builds on the single-thruster softstart was demonstrated to be simple, benign to the power system, and repeatable. Shutdowns were also similarly demonstrated. Multi-thruster control across the array power-voltage curve was accomplished in the same way as single-thruster control, by adjusting thruster mass flow rates and magnet currents. Rapid throttling of adjacent thrusters in opposite directions of power did not demonstrably stress the system. Stable dual-thruster operation was demonstrated at power levels up to 10 kW.

Operation of cathodes connected electrically in parallel was demonstrated. Four experimental "knobs" were shown to have an effect on the relative amounts of discharge current emitted by each cathode: the heater current, keeper current, mass flow rate, and added ballast resistance. While the heater and keeper currents did affect the cathode current sharing, they appeared to have slow response time, non-linear response, and relatively poor control authority over the test conditions investigated. The amount of added ballast resistance also affected current sharing, but this decreases the system efficiency and does not provide an attractive solution for active system control. The best control method was found to be using the cathode mass flow rates, where nearly equal discharge current sharing was controlled over a wide range of throttle conditions. During all of these tests with laboratory cathodes, it appeared that differences in laboratory cathode geometry and total cathode leg resistance could have been driving some of the results.

Cathode current sharing was also investigated in a series of tests using identical Dawn flight-spare discharge cathodes. Additionally, implementation of different ballast resistors with finer control meant that tests could be performed with equal total resistances in the two cathode legs. With these changes, cathode current sharing control was demonstrated using identical thruster operating conditions by changing cathode flow rates in lock-step. Equal sharing was observed only over a small range of cathode flow rates that was independent of cathode leg resistance. A relationship between cathode current sharing and cathode coupling potential was observed whereby the dominant cathode has a coupling behavior similar to single-thruster operation, and the other cathode has a markedly different behavior. Finally, it was shown that the range of cathode flow rates required for equal current sharing is a function of anode flow rate. Although the physical processes underlying these current sharing behaviors need more investigation, it has been demonstrated that control of cathode sharing is possible and that direct-drive architectures utilizing dual-parallel thrusters with individual cathodes are feasible.

Finally, the multi-thruster work described in this paper was conducted in part to address the technical issues identified in Table 1. The present status of those issues, derived from the results of the testing, is shown in Table 2.

Table 2. Present Status of Investigation of Dual-Thruster Direct-Drive Technical Issues.

1	How do you start, stop, and operate multiple Hall thrusters in a direct-drive system?	Same as for a single-thruster system. Demonstrated second thruster softstart and shutdown while first thruster was operating.
2	How do you operate near the peak power point with multiple thrusters?	Same as for a single-thruster system. The total system flowrate drives the operation on the solar array power-voltage curve.
3	What additional filtering is necessary when operating multiple thrusters in parallel?	No additional filtering was necessary.
4	Is current sharing possible with all of the cathodes tied together?	Yes. Demonstrated at power levels up to 10 kW.
5	How do you enforce cathode current sharing for multiple Hall thrusters in a direct-drive system?	Can be accomplished with adjustment of cathode mass flow rates.

Acknowledgments

The work described in this paper was carried out by the Jet Propulsion Laboratory, California Institute of Technology, under a contract with the National Aeronautics and Space Administration. Funding for this work was provided by the NASA Office of the Chief Technologist In-Space Propulsion Project. The NASA 173M thrusters were loaned by Hani Kamhawi of NASA Glenn Research Center. Thanks to Rich Hofer of JPL for guidance in use of the thrusters, and to Ray Swindlehurst and Nowell Niblett of JPL for their contributions to test setup and operation.

References

1. Hamley, J.A., J.M. Sankovic, J.R. Miller, M.J. O'Neill, P. Lynn, and S.R. Oleson, "Hall Thruster Direct Drive Demonstration," AIAA 1997-2787, 33rd Joint Propulsion Conference, Seattle, WA, July 6-9, 1997.
2. Jongeward, G.A., I. Katz, I.G. Mikellides, M.R. Carruth, E.L. Ralph, D.Q. King, and T. Peterson, "High Voltage Solar Arrays for a Direct Drive Hall Effect Propulsion System," IEPC 2001-0327, 27th International Electric Propulsion Conference, Pasadena, CA, Oct. 15-19, 2001.
3. Hoskins, W.A., D. Homiak, R.J. Cassady, T. Kerslake, T. Peterson, D. Ferguson, D. Snyder, I.G. Mikellides, G.A. Jongeward, T. Schneider, and M. Hovater, "Direct Drive Hall Thruster System Development," AIAA 2003-4726, 39th Joint Propulsion Conference, Huntsville, AL, July 20-23, 2003.
4. Dankanich, J.W., "Direct Drive for Low Power Hall Thrusters," AIAA 2005-4118, 41st Joint Propulsion Conference, Tucson, AZ, July 10-13, 2005.
5. Aintablian, H.O., H. Kirkham, and P. Timmerman, "High Power, High Voltage Electric Power System for Electric Propulsion," AIAA 2006-4134, 4th International Energy Conversion Conference, San Diego, CA, June 26-29, 2006.
6. Brandhorst Jr., H.W., S.R. Best, J.A. Rodiek, M.J. O'Neill, and M.F. Piszczor, "Direct-Drive Performance of a T-100 HET powered by Triple Junction, High-Voltage Concentrator PV Array," AIAA 2010-6620, 46th Joint Propulsion Conference, Nashville, TN, July 25-28, 2010.
7. Brophy, J.R., R. Gershman, N. Strange, D. Landau, R.G. Merrill, and T. Kerslake, "300-kW Solar Electric Propulsion System Configuration for Human Exploration of Near-Earth Asteroids," AIAA 2011-5514, 47th Joint Propulsion Conference, San Diego, CA, July 31 - Aug. 3, 2011.
8. Mercer, C.R., S.R. Oleson, E.J. Pencil, M.F. Piszczor, L.S. Mason, K.M. Bury, D.H. Manzella, T.W. Kerslake, J.S. Hojnicki, and J.R. Brophy, "Benefits of Power and Propulsion Technology for a Piloted Electric Vehicle to an Asteroid," AIAA 2011-7252, AIAA SPACE 2011 Conference, Long Beach, CA,
9. Snyder, J.S., J.R. Brophy, R.R. Hofer, D.M. Goebel, and I. Katz, "Experimental Investigation of a Direct-Drive Hall Thruster and Solar Array System at Power Levels up to 10 kW," AIAA 2012-4068, 48th Joint Propulsion Conference, Atlanta, GA, 30 July - 01 August, 2012.
10. Brophy, J.R., "Near-Earth Asteroid Retrieval Mission (ARM) Study," IEPC 2013-082, to be presented at the 33rd International Electric Propulsion Conference, Washington, D.C., Oct. 7-10, 2013.
11. Hofer, R.R. and T.M. Randolph, "Mass and Cost Model for Selecting Thruster Size in Electric Propulsion Systems," *Journal of Propulsion and Power*, 2013. **29**(1): p. 166-177.
12. Stella, P.M., S. DiStefano, M.D. Rayman, and A. Ulloa-Severino, "Early mission power assessment of the Dawn solar array," in *Proceedings of the 34th IEEE Photovoltaic Specialists Conference*, Philadelphia, PA, 2009.

13. Rayman, M.D., T.C. Fraschetti, C.A. Raymond, and C.T. Russell, "Coupling of system resource margins through the use of electric propulsion: Implications in preparing for the Dawn mission to Ceres and Vesta," *Acta Astronautica*, 2007. **60**(10-11): p. 930-938.
14. Cardell, G., A. Ulloa-Severion, and M. Gross, "The Design and Operation of the Dawn Power System," AIAA 2012-3898, 10th International Energy Conversion Engineering Conference, Atlanta, GA, 30 July - 01 August, 2012.
15. Kerslake, W.R. and S. Domitz, "Neutralization Tests on the SERT II Spacecraft," AIAA 79-2064, 14th International Electric Propulsion Conference, Princeton, NJ, Oct. 30 - Nov. 1, 1979.
16. Rusakov, A.V., A.V. Kochergin, A.V. Semenkin, S.O. Tverdokhlebov, and V.I. Garkusha, "Multiple Thruster Propulsion Systems Integration Study," IEPC 97-130, 25th International Electric Propulsion Conference, Cleveland, OH, Oct. 1997.
17. Zakharenkov, L.E., A.V. Semenkin, A.V. Rusakov, N.A. Urchenko, S.O. Tverdokhlebov, V.I. Garkusha, U.V. Lebedev, S.N. Podkolsin, and J.M. Five, "Study of Multi-Thruster Assembly Operation," IEPC 2003-311, 28th International Electric Propulsion Conference, Toulouse, France, March 17-21, 2003.
18. Spores, R.A., G.G. Spanjers, M. Birkan, and T.J. Lawrence, "Overview of the USAF Electric Propulsion Program," AIAA 2001-3225, 37th Joint Propulsion Conference, Salt Lake City, UT, July 8-11, 2001.
19. Walker, M.L.R. and A.D. Gallimore, "Hall Thruster Cluster Operation with a Shared Cathode," *Journal of Propulsion and Power*, 2007. **23**(3): p. 528-536.
20. Beal, B.E., A.D. Gallimore, and W.A. Hargus Jr., "Effects of Cathode Configuration on Hall Thruster Cluster Plume Properties," *Journal of Propulsion and Power*, 2007. **23**(4): p. 836-844.
21. Beal, B.E., *Clustering of Hall Effect Thrusters for High-Power Electric Propulsion Applications*, Ph.D. Dissertation, University of Michigan, 2004.
22. Shimada, S., Y. Gotoh, E. Nishada, H. Takegahara, K. Nakamaru, H. Nagano, and K. Terada, "Evaluation of Ion Thruster Beam Neutralization," IEPC 1991-025, 22nd Electric Propulsion Conference, Viareggio, Italy, Oct. 1991.
23. Shimada, S., K. Satoh, Y. Gotoh, E. Nishida, I. Terukina, T. Noro, H. Takegahara, K. Nakamaru, and H. Nagano, "Development of Ion Engine System for ETS-VI," IEPC 1993-009, 23rd International Electric Propulsion Conference, Seattle, WA, Sept. 1993.
24. Nagano, H., K. Kajiwara, Y. Gotoh, E. Nishida, and Y. Fujita, "On-Orbit Performance of ETS-VI Ion Engine Subsystem," IEPC 1995-139, 24th International Electric Propulsion Conference, Moscow, Russia, Sept. 1995.
25. Hargus Jr., W.A. and G. Reed, "The Air Force Clustered Hall Thruster Program," AIAA 2002-3678, 38th Joint Propulsion Conference, Indianapolis, IN, July 7-10, 2002.
26. Esram, T. and P.L. Chapman, "Comparison of Photovoltaic Array Maximum Power Point Tracking Techniques," *IEEE Transactions on Energy Conversion*, 2007. **22**(2): p. 439-449.
27. Hohm, D.P. and M.E. Ropp, "Comparative Study of Maximum Power Point Tracking Algorithms," *Progress in Photovoltaics: Research and Applications*, 2003. **11**(1): p. 47-62.
28. Snyder, J.S., T.M. Randolph, D.F. Landau, K.M. Bury, S.P. Malone, and T.A. Hickman, "Power and Propulsion System Design for Near-Earth Object Robotic Exploration," AIAA 2011-5662, 47th Joint Propulsion Conference, San Diego, CA, July 31 - Aug. 3, 2011.
29. Canadian Solar, Inc., *CS5P-240/245/250/255/260M Datasheet*. Available from: www.canadiansolar.com/dl.php?dir=datasheets&file=CS5P-M_en.pdf [Cited May, 2012].
30. Hofer, R.R., R.S. jankovsky, and A.D. Gallimore, "High-Specific Impulse Hall Thrusters, Part 1: Influence of Current Density and Magnetic Field," *Journal of Propulsion and Power*, 2006. **22**(4): p. 721-731.
31. Personal Communication, Hofer, R.R., Jet Propulsion Laboratory, June 2012.
32. Christensen, J.A., K.J. Freick, D.J. Hamel, S.L. Hart, K.T. Norenberg, T.W. Haag, M.J. Patterson, V.K. Rawlin, and J. Sovey, "Design and Fabrication of a Flight Model 2.3 kW Ion Thruster for

the Deep Space 1 Mission," AIAA 98-3327, 34th Joint Propulsion Conference, Cleveland, OH, July 13-15, 1998.
33. Brophy, J.R., C.E. Garner, and S. Mikes, "Dawn Ion Propulsion System - Initial Checkout after Launch," AIAA 2008-4917, 44th Joint Propulsion Conference, Hartford, CT, July 2008.
34. Hofer, R.R., *Development and Characterization of High-Efficiency, High-Specific Impulse Xenon Hall Thrusters*, NASA/CR-2004-213099, University of Michigan, Ann Arbor, MI, June 2004.
35. Chu, L.E., J.S. Snyder, D.M. Goebel, and R.E. Wirz, "Experimental Investigation of Cathode Current Sharing in Parallel Discharges," IEPC 2013-069, to be presented at the 33rd International Electric Propulsion Conference, Washington, D.C., Oct. 6-10, 2013.